ACS APPLIED MATERIALS & INTERFACES

Research Article

www.acsami.org

# One-Step Process for the Synthesis and Deposition of Anatase, Two-Dimensional, Disk-Shaped $TiO_2$ for Dye-Sensitized Solar Cells

Chang Soo Lee, Jin Kyu Kim, Jung Yup Lim, and Jong Hak Kim*

Department of Chemical and Biomolecular Engineering, Yonsei University, 262 Seongsanno, Seodaemun-gu, Seoul 120-749, South Korea

Supporting Information

**ABSTRACT:** We report a one-step process for the synthesis and deposition of anatase, two-dimensional (2D), disk-shaped $TiO_2$ (DS-$TiO_2$) using titanium isopropoxide (TTIP), ethyl cellulose (EC), and solvents. The planar structure of EC plays a pivotal role as the sacrificing template to generate the 2D disk-shaped structure with a thickness of 1.5−3.5 $\mu$m, while a disk-like structure was well developed in the tetrahydrofuran (THF)/toluene mixed solvent. The quasi-solid-state dye-sensitized solar cells (qssDSSCs), fabricated with a nanogel electrolyte and a DS-$TiO_2$ layer on a nanocrystalline (NC)-$TiO_2$ photoanode, showed an energy conversion efficiency of 5.0% without any $TiCl_4$ post-treatment, which is higher than that fabricated without DS-$TiO_2$ (4.2%). When utilizing a poly((1-(4-ethenylphenyl)methyl)-3-butyl-imidazolium iodide) (PEBII) as the solid electrolyte, a high efficiency of 6.6% was achieved due to the combination of high mobility PEBII and a bifunctional DS-$TiO_2$ layer with a 2D structure and anatase phase. The bifunctionality of the DS-$TiO_2$ layer allows greater light scattering back into the device and provides additional surface area for improved dye adsorption, resulting in short circuit current density ($J_{sc}$).

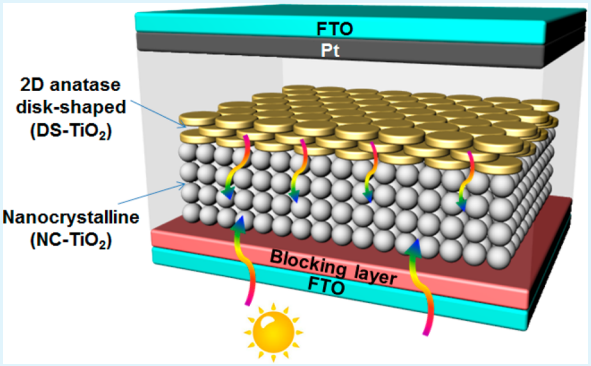


**KEYWORDS:** *dye-sensitized solar cell (DSSC), titanium dioxide ($TiO_2$), two-dimensional (2D), disk-shaped structure, ethyl cellulose*

## INTRODUCTION

Recently, as global warming has intensified, more attention has been focused on sustainable and renewable energy sources. Among them, dye-sensitized solar cells (DSSCs) first reported by M. Gratzel in 1991 have attracted enormous interest as promising future energy devices due to their low-cost, simple fabrication method, and remarkable power conversion efficiency.[1] Much of the current research has been focused on improving the device efficiency, which has been obtained through development of a novel dye,[2] a nanocrystalline $TiO_2$ photoanode,[3−6] transparent conducting oxide (TCO),[7] electrolyte,[8−10] or counter electrode.[11] Among these, the $TiO_2$ photoanode is considered a pivotal element because it can directly affect light harvesting, charge recombination, and interfacial contact of the electrode/electrolyte.

In general, the photoanodes of DSSCs are composed of fluorine-doped tin oxide (FTO) glass, a blocking layer that prevents recombination of electrons between electrolyte and FTO glass, and a nanocrystalline $TiO_2$ layer for dye adsorption. Although a dye-adsorbed nanocrystalline $TiO_2$ layer has been commonly used as a photoanode of DSSCs, it has some disadvantages such as lower conductivity and light scattering effect due to its less organized particulate structure. To improve the light harvesting properties, many groups have developed methods to fabricate light scattering particles, which are then deposited directly onto the nanocrystalline $TiO_2$ layer to reflect unutilized light. The light scattering ability of the photoelectrode plays an important role in efficient excitation of electrons and thus improved energy conversion efficiencies in DSSCs, mostly due to the improved short circuit current density ($J_{sc}$) value.

Recently, there have been many studies related to the enhancement of the light scattering abilities of photoelectrodes by employing various methods, structures, and materials mostly based on three-dimensional (3D) structures.[12−27] Large $TiO_2$ particles (typically >200 nm) have been typically analyzed for formation of the scattering layer, because they reflect light much more efficiently than nanoparticles, smaller than 20 nm.[15,16] For example, anatase-phased $TiO_2$ beads with a large particle size have been researched as a light scattering layer due to their dual-functional properties, improved light scattering ability, and increased amount of dye loading.[17−19] Other metal oxides have also been researched to enhance the light scattering ability, such as a ZnO hemisphere array to increase the light reflecting behavior below the nanocrystalline $TiO_2$ layer, demonstrating a conversion efficiency of 11%.[20] The quintuple-shelled $SnO_2$ hollow sphere was synthesized by employing a sacrificial template that was highly advantageous

Received: August 6, 2014
Accepted: November 14, 2014
Published: November 14, 2014

  

due to its light scattering property and faster electron transfer rate.[21,22] Moreover, a $SnO_2$ core and $TiO_2$ shell structure was fabricated to achieve appropriate conduction and valence band energy level.[23] In addition, a variety of novel $TiO_2$ structures suitable for the light scattering layer have been reported with different synthetic methods. The anatase-phase, sugar apple-shaped $TiO_2$ sphere was synthesized by hydrothermal reaction, and the conversion efficiency of the DSSC was close to 7.2% after $TiCl_4$ treatment.[24] Rutile-phase flower-like $TiO_2$ nanospheres were also synthesized using a block-graft copolymer containing a $TiO_2$ source and exhibited significant light scattering ability.[25] Also, it was confirmed that perpendicular $TiO_2$ nanotube arrays show outstanding properties in terms of better light scattering properties and faster electron transfer compared to nanocrystalline structures.[26,27]

Although the 3D nanostructured metal oxides are highly effective in improving light scattering abilities, their synthesis processes are usually complicated and quite expensive. First, such nanostructured metal oxides are generally based on a hydrothermal reaction at high temperature or an inverse opal structure, using expensive well-defined monodisperse polystyrene as a template.[28] Second, the preparation of a scattering layer should be sequentially followed by deposition onto the nanocrystalline $TiO_2$ layer using an appropriate polymer binder to increase the viscosity. Finally, an annealing process at a high temperature such as 450 °C is required, implying that the synthesis and deposition of the metal oxide scattering layer should be separated into a two-step process. A variety of one-dimensional (1D) $TiO_2$ nanostructures has been reported, including nanorods,[29,30] nanotubes,[31,32] and nanowires.[33,34] However, there have been no reports about two-dimensional (2D), disk-shaped $TiO_2$ structures with an anatase phase. The 2D nanostructures would be advantageous in terms of electron diffusion path and light reflecting ability because of the efficient stacking of 2D particles.[35]

Hence, in this work, we report a one-step process for the synthesis and deposition of anatase, 2D, disk-shaped $TiO_2$ (DS-$TiO_2$) using only titanium isopropoxide (TTIP), ethyl cellulose (EC), and solvents. EC, a polysaccharide with a planar structure, was employed as the template to synthesize the DS-$TiO_2$ directly on the nanocrystalline $TiO_2$ layer as a light scattering layer. The structure and morphology of the DS-$TiO_2$ layer were characterized using field emission scanning electron microscopy (FE-SEM), energy-filtering transmission electron microscopy (EF-TEM), and X-ray diffraction (XRD). The light reflecting ability and light harvesting efficiency of the DSSCs with DS-$TiO_2$ film were characterized by UV−visible reflectance, current density−voltage (J-V) curves, incident photon-to-electron conversion efficiency (IPCE), and electrochemical impedance spectroscopy (EIS) measurements.

## EXPERIMENTAL SECTION

**Materials.** Ethyl cellulose (EC, 48% ethoxyl), titanium isopropoxide (TTIP, 97%), hydrochloric acid (HCl, 37%), titanium diisopropoxide bis(acetylacetonate) (75 wt % in isopropanol), chloroplatinic acid hexahydrate ($H_2PtCl_6$, ≥ 37.50% Pt basis), 1-methyl-3-propylimidazolium iodide (MPII), silica (fumed, $SiO_2$, 7 nm), iodine ($I_2$, ≥99%), poly(ethylene glycol) dimethyl ether (PEGDME, $M_n$ ~ 500 g/mol), and sodium hydroxide (NaOH, ≥ 97.0%, pellets) were all purchased from Sigma-Aldrich and used as received without purification.

**One-Step Process for the Synthesis and Deposition of DS-$TiO_2$.** First, 0.4 g of EC was dissolved in 2 mL of THF (Daejung) and 0.4 mL of toluene (JT Baker) to produce a highly viscous and transparent solution. Separately, the TTIP sol−gel solution was prepared by slowly dropping HCl into TTIP at a volume ratio of 2:1 (TTIP:HCl) under vigorous stirring. After aging for 30 min, 0.3, 0.45, and 0.6 mL of as-prepared TTIP sol−gel solutions were dropped into an EC solution, named DS1, DS2, and DS3, respectively. The solutions were further stirred for 6 h at room temperature to produce a viscous paste. After direct doctor-blading of the viscous paste onto the substrate, the samples were dried at 50 or 80 °C for 1 h and then calcined at 450 °C for 30 min to generate the anatase DS-$TiO_2$ structure with a thickness of 2−3 $\mu$m.

**Fabrication of DSSCs.** Quasi-solid-state DSSCs (qssDSSCs) and solid-state DSSCs (ssDSSCs) with an active area of 0.16 $cm^2$ were fabricated according to the following procedure.[36−41] In order to prepare the photoanode and counter electrode, fluorine-doped tin oxide (FTO, Pilkington Co., LtD.) glass was employed as a transparent conductive oxide (TCO) glass substrate. The photoanodes were prepared by deposition of a thin blocking layer to prevent recombination between the electrolyte and FTO glass. Titanium diisopropoxide bis(acetylacetonate) was diluted with butanol, spin-coated onto the FTO glass, and gradually heated and sintered at 450 °C for 30 min. Then, commercially available $TiO_2$ paste (Dyesol, 18NR-T) was coated onto the $TiO_2$ blocking layer using the doctor-blade technique, dried at 50 or 80 °C in an oven for 1 h, and calcined at 450 °C to produce an approximately 7-$\mu$m-thick NC-$TiO_2$ layer. For application of DS-$TiO_2$ to the light scattering layer, the viscous paste was directly doctor-bladed onto the NC layer and calcined at 450 °C for 30 min. The prepared photoanodes were immersed overnight in a $10^{-4}$ M $Ru(dcbpy)_2(NCS)_2$ dye (dcbpy =2,2-bipyridyl-4,4-dicarboxylato) N719 solution in absolute ethanol to sensitize the $TiO_2$ photoanodes. For the preparation of the counter electrodes, 1 wt % $H_2PtCl_6$ solutions in isopropanol were spin-coated onto FTO glasses and sintered at 450 °C for 30 min. Finally, the quasi-solid-state polymer electrolytes were prepared by dissolving PEGDME, $SiO_2$, MPII, and $I_2$ in acetonitrile under vigorous stirring, according to our previously reported method.[31,32] The polymer electrolyte solutions in acetonitrile were directly cast onto the photoanodes. Poly((1-(4-ethenylphenyl)methyl)-3-butyl-imidazolium iodide) (PEBII) was used as the solid-state polymerized ionic liquid (PIL) without any additives.[36−40] Both electrodes were then superimposed and pressed between two glass plates in order to achieve slow evaporation of the solvent and a thin electrolyte layer. The cells were placed in a vacuum oven for 1 day to allow complete evaporation of the solvent.

To evaluate the photoelectrochemical performance, we employed J-V measurements in order to obtain the short-circuit current ($J_{sc}$, mA/$cm^2$), open-circuit voltage ($V_{oc}$, V), fill factor (FF), and energy conversion efficiency ($\eta$, %). Those variables were measured using a Keithley Model 2400 and a 1,000 W xenon lamp (Oriel, 91193). The light intensity was homogeneous over an 8 in. × 8 in. area and was calibrated using a Si solar cell (Fraunhofer Institute for Solar Energy System, Mono-Si + KG filter, Certificate No. C-ISE269) with a sunlight intensity of one (100 mW/$cm^2$), which was verified by a NREL-calibrated Si solar cell (PV Measurements Inc.).

**Measurement of Dye Adsorption.** The N719 dye-sensitized $TiO_2$ photoelectrode with an active area of 0.49 $cm^2$ was dipped into 5.0 mL of a 0.1 M NaOH solution in the mixed solvent of ethanol and deionized water (1:1 volume ratio). The resulting solution was further stirred until the NaOH solution provided complete desorption of N719 dye from the photoelectrode. Then, N719 dye adsorption was calculated using the UV−visible spectroscopy adsorption peak value at 515 nm, according to the Beer−Lambert law, as shown in the following equation

$$A = \varepsilon lc \quad (1)$$

Here, $A$ is the absorbance of the UV−visible spectra at 515 nm, $\varepsilon$ = 14,100/M cm is the molar extinction coefficient of N719 dye at 515 nm, $l$ is the path length of the light beam, and $c$ is the dye concentration.

**Characterization.** The morphology of the $TiO_2$ films was characterized by field-emission scanning electron microscopy (FE-SEM, SUPRA 55VP, Carl Zeiss, Germany) and energy-filtering

**Scheme 1. Schematic of the Synthesis of 2D Disk-Shaped $TiO_2$ Using TTIP, EC, and a THF/Toluene Mixed Solvent**

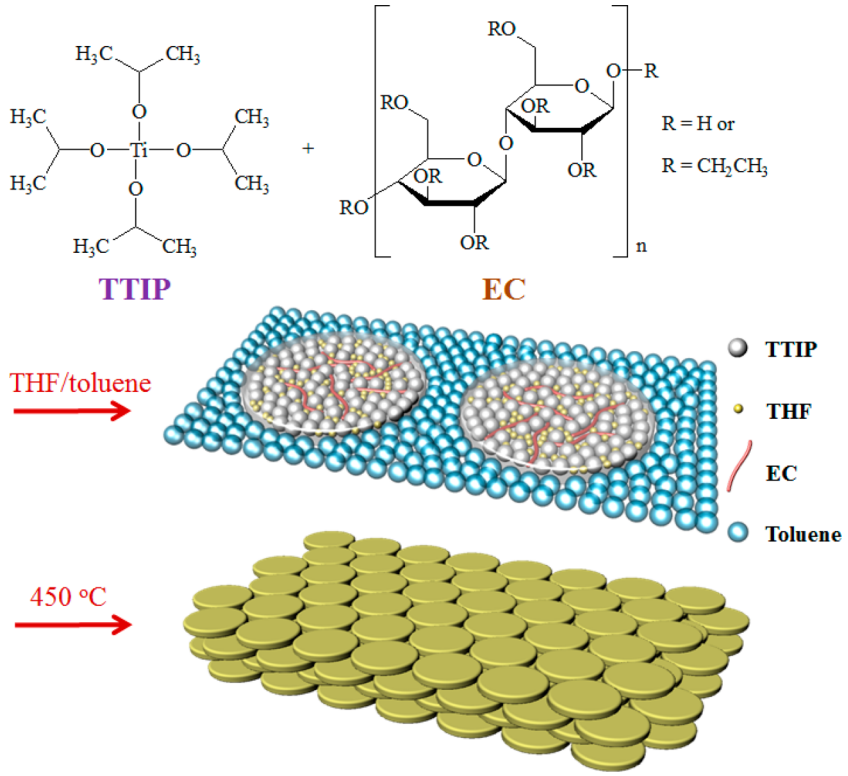


transmission electron microscopy (EF-TEM, Philips CM30) operated at 120 kV. The XRD spectra were measured by a Rigaku RINT2000 wide-angle goniometer with a Cu cathode operated at 40 kV and 300 mA. The concentration of the adsorbed dye and the reflectance spectra were measured as a function of wavelength from 300 to 800 nm using a UV–visible spectrophotometer (Hewlett-Packard, Hayward, CF). The incident photo to current conversion efficiency (IPCE) was measured from 300 to 800 nm (McScience, K3100).

## RESULTS AND DISCUSSION

A facile, effective method was developed to synthesize DS-$TiO_2$ with a 2D structure and anatase phase using EC as a template through the control of specific interactions between the polymer/$TiO_2$ hybrids and the solvents (Scheme 1). The 2D organized structure is expected to be an excellent candidate scattering layer in DSSCs[35] because it could improve light scattering properties without any negative impact on the electrolyte pore-filling, which will be discussed in the next sections. As shown in Figures 1a and b, a 2D disk-shaped structure was not obtained when prepared without EC, irrespective of the type of solvent. This demonstrates that the EC polymer plays a pivotal role as a structure-directing agent due to its well-defined, 2D planar structure. There were no noticeable pores in the structure when prepared using THF as a solvent, while the use of a THF/toluene mixture resulted in the generation of pores with irregular shapes. This result is obtained because TTIP has good solubility in THF, allowing it to spread well and resulting in a uniform film structure without any pores. However, the solubility of TTIP decreases with the addition of toluene due to the poor interaction of polar TTIP with nonpolar toluene, leading to aggregation of TTIP. The interstitial spaces among the aggregated TTIP domains produce pores upon calcination. This demonstrates that the balanced interaction between the titania precursor and the solvent is a critical factor in generating the pore structures.

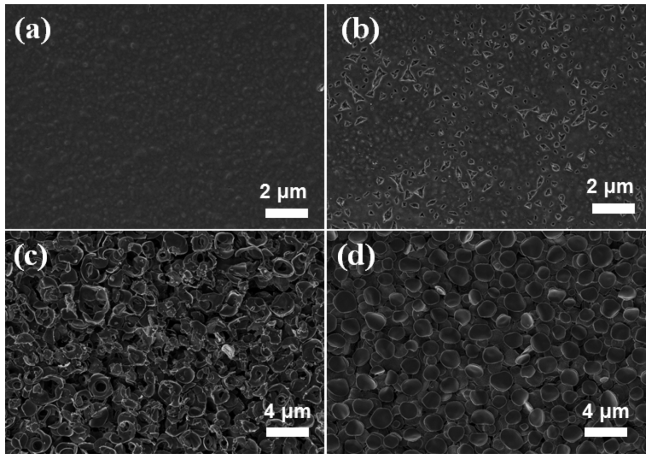


**Figure 1.** FE-SEM images of $TiO_2$ prepared directly on FTO substrates via spin-coating using (a) THF only (without EC), (b) a THF/toluene mixture (without EC), (c) THF only (with EC), and (d) a THF/toluene mixture (with EC).

When prepared using EC, a 2D planar structure was obtained and further well-developed upon using the THF/toluene mixture as the solvent, as shown in Figures 1c and d. To the best of our knowledge, this is the first report of the synthesis of a 2D disk-shaped $TiO_2$ structure with an anatase phase. This structure results from the effective role of EC as a structure-directing agent to generate a 2D planar structure, which is presumably formed due to strong hydrogen bonding interactions in the linear direction of the EC plane and the perpendicular arrangement of the C–H–O bonds in EC.[42−45] The high molecular weight and hydrophilicity of EC are other

important factors in increasing the viscosity of the solution when combined with TTIP. This allows for the direct use of the doctor-blade method, which is a well-known, established technique to obtain appropriate $TiO_2$ film thickness. TTIP is a small, hydrophilic titania precursor and thus provides preferential interactions with the hydrophilic EC polymer chains. Thus, the EC functions as a structure-directing agent not only on the mesoscopic scale via self-assembly of EC/$TiO_2$ hybrids but also in the macroscopic crystal growth of $TiO_2$.

Careful tuning of the polymer−solvent interactions is responsible for the generation of 2D disk-shaped structures with a uniform shape and size. Toluene is a water-immiscible, nonpolar, monosubstituted benzene derivative and thus is a poor solvent for the hydrophilic EC chains as well as the polar TTIP precursor. Therefore, the interfacial energy between the EC/TTIP hybrids and solvent increases with increasing toluene content, leading to decreased volume of the EC/TTIP domains and a mesoscopic self-aggregated structure and eventual production of a well-defined, 2D disk-shaped morphology. Addition of 0.4 mL of toluene to 0.4 g of EC dissolved in 2 mL of THF was needed to achieve the critical concentration for the miscibility limit of the EC/THF/toluene system, above which macrophase separation occurs. As shown in Figure S1, the EC/TTIP sol−gel solution became opaque with the addition of toluene, indicating the progress of macrophase separation. In summary, the preparation of novel 2D, disk-shaped $TiO_2$ in large quantities was possible due to three important factors: 1) the planar structure of EC, 2) control of the interaction between EC/TTIP hybrids and solvent, and 3) use of the doctor-blading method due to the high viscosity of the solution.

The ratio of TTIP to EC in the solution is another parameter that affects the size of DS-$TiO_2$, as shown in Figure 2, where the amount of TTIP solution was varied between 0.3, 0.45, and 0.6 mL for DS1, DS2, and DS3, respectively. The average size of the DS-$TiO_2$ particles increased with increasing amount of TTIP solution, which was also supported by the EF-TEM images shown in Figure S2. All of the DS-$TiO_2$ layers were directly and uniformly deposited onto the 7-$\mu$m-thick nanocrystalline (NC) $TiO_2$ layer via a one-step doctor blading method, as shown in Figure 3. The DS-$TiO_2$ layers had sufficient space for the polymer electrolyte to deeply penetrate into the $TiO_2$ mesopores. The thickness of DS1-$TiO_2$, DS2-$TiO_2$, and DS3-$TiO_2$ layer was approximately 1.5, 2.5, and 3.5 $\mu$m, respectively. This shows that, as the amount of TTIP solution increased, the thickness of the DS-$TiO_2$ layer increased gradually, which is also important in improving the light scattering properties. With more TTIP in the solution, concentration of the solid-forming phase in the paste becomes higher, resulting in an increased film thickness after evaporation of the solvent and calcination at 450 °C. However, the use of an excess amount of TTIP solution resulted in fragility of the DS-$TiO_2$ layer (DS3, Figures 2e and f), which may have a negative impact on device performance.

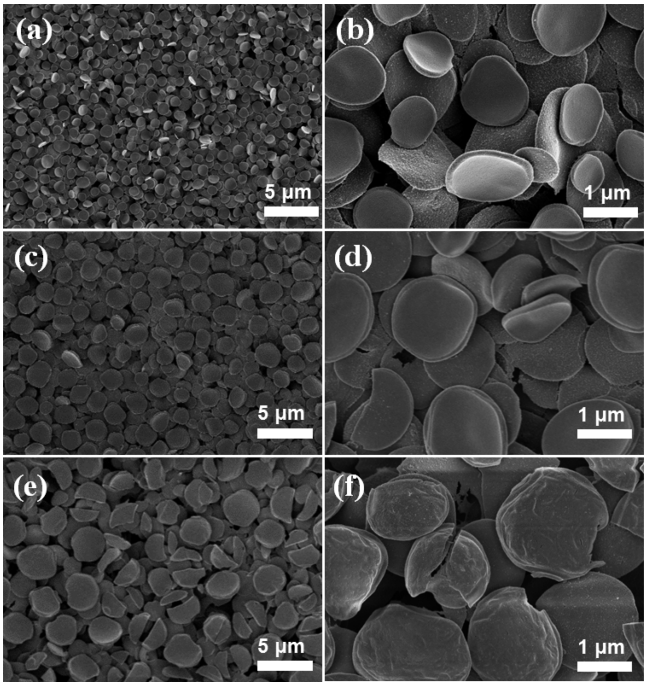


**Figure 2.** FE-SEM surface images of DS-$TiO_2$: (a, b) DS1, (c, d) DS2, and (e, f) DS3.

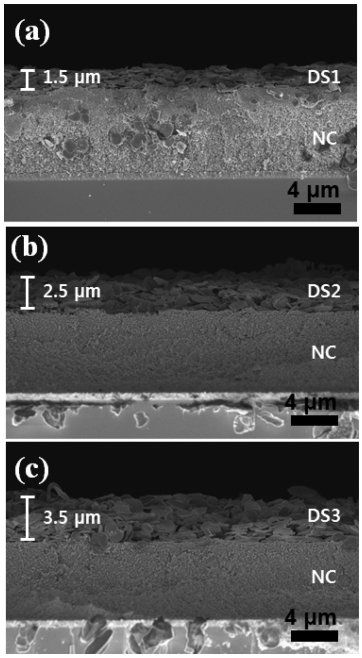


**Figure 3.** Cross-sectional FE-SEM images of DS-$TiO_2$ on NC-$TiO_2$/FTO photoanodes: (a) DS1, (b) DS2, and (c) DS3.

A large amount of DS-$TiO_2$ powder was obtained by scraping the DS-$TiO_2$ film from FTO glass for XRD characterization, which was possible due to the large film thickness resulting from the high viscosity of the solution. As shown in Figure 4a, several strong sharp peaks appeared at 2$\theta$ values of 25.3°, 37.8°, 48.1°, 54.0°, 55.0°, 62.7°, 69.1°, and 75.1°, which are assigned to the anatase planes of (101), (004), (200), (105), (211), (115), (220), and (215), respectively. Thus, the DS-$TiO_2$ particles were all structured as a pure anatase crystalline phase. The 2D anatase phase $TiO_2$ materials are characterized in terms of the adsorption of N719 dye and light scattering, which are important factors in determining the power conversion efficiency.

UV−visible absorption spectroscopy was employed to investigate the effect of the DS-$TiO_2$ layer on dye adsorption, as shown in Figure 4b. When the DS-$TiO_2$ was deposited onto a NC-$TiO_2$ film as a top light scattering layer, the dye adsorption was increased compared to that of the neat NC

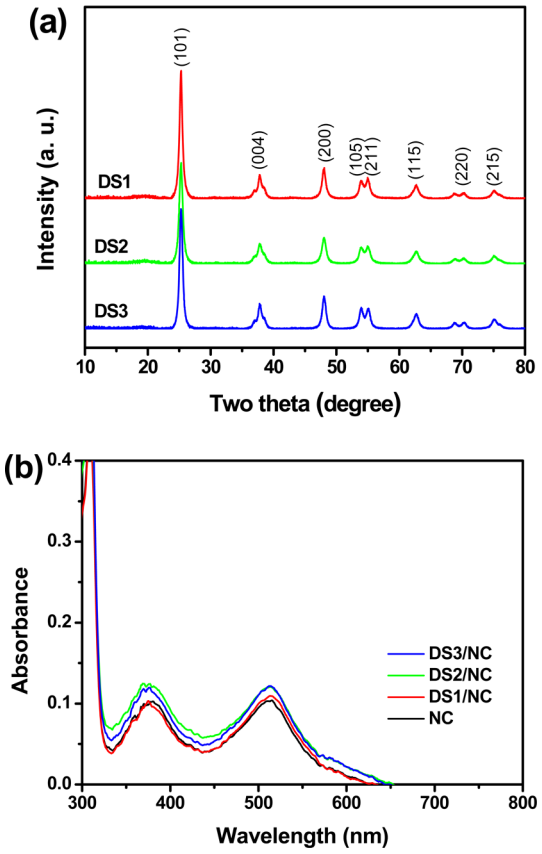


**Figure 4.** (a) XRD patterns of DS-$TiO_2$ powders after calcination at 450 °C and (b) UV–vis adsorption spectra of various photoanodes used for measuring dye adsorption.

layer due to increased film thickness. In particular, DS2 and DS3-$TiO_2$ were more effective than DS1-$TiO_2$ due to their greater film thickness, as revealed by the cross-sectional FE-SEM images. However, there was no significant difference in the dye loadings between DS2/NC-$TiO_2$ and DS3/NC-$TiO_2$ (Table 1), implying negligible effect of film thickness, i.e., 9.5 $\mu$m (=7 + 2.5) vs 10.5 $\mu$m (=7 + 3.5). It should be noted that the energy conversion efficiency of the NC-$TiO_2$-based cell (a control group) without a scattering layer was not significantly changed when the $TiO_2$ film thickness was between 7 and 12 $\mu$m (Table 1, Figure 6b). This is because the increased dye loading with the increased film thickness was compensated by the longer electron diffusion path, as well as the difficulties of electrolyte pore-filling, resulting in the reduced $V_{oc}$ value.

**Table 1. Performance of qssDSSCs Fabricated with a Nanogel and the Different Photoanodes under One Sun Illumination Conditions (at 100 mW/cm$^2$) and ssDSSC Fabricated with a Solid PIL Electrolyte**

| photoanode | $V_{oc}$ (V) | $J_{sc}$ (mA/cm$^2$) | FF | $\eta$ (%) | dye loading (nmol/cm$^2$) |
|---|---|---|---|---|---|
| NC (7 $\mu$m) | 0.69 | 10.7 | 0.58 | 4.2 | 74.4 |
| NC (12 $\mu$m) | 0.64 | 10.3 | 0.60 | 4.0 | |
| DS1/NC | 0.68 | 11.4 | 0.58 | 4.6 | 79.7 |
| DS2/NC | 0.68 | 12.9 | 0.58 | 5.0 | 86.1 |
| DS3/NC | 0.68 | 12.7 | 0.57 | 4.9 | 86.2 |
| DS2/NC (PIL) | 0.79 | 13.0 | 0.65 | 6.6 | |

The performance of DSSCs is also strongly dependent on the light scattering ability of the photoanode. Thus, the light reflecting ability of the DS-$TiO_2$ layer was measured using UV–visible reflectance spectroscopy as a function of wavelength between 300 to 800 nm, as shown in Figure 5a. The reflectance

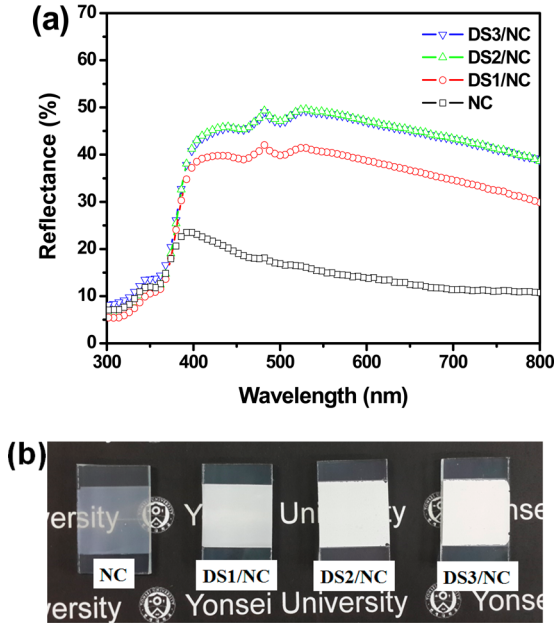


**Figure 5.** (a) UV–visible reflectance spectra and (b) photos of photoanodes of NC-$TiO_2$, DS1 on NC-$TiO_2$, DS2 on NC-$TiO_2$, and DS3 on NC-$TiO_2$.

spectra of DS-$TiO_2$ on the NC photoanodes were always higher than that of the NC-only photoanode over the entire measured wavelength range. In particular, the obtained reflectance values of the photoanodes demonstrated the following order: DS3/NC ≅ DS2/NC > DS1/NC ≫ only NC. This sequence is consistent with the sizes and film thicknesses of DS-$TiO_2$, with larger DS-$TiO_2$ particle size (or greater DS-$TiO_2$ film thickness) corresponding to greater reflectance. Thus, the thickness and particle size of the DS-$TiO_2$ layer are important factors in determining the light reflecting ability. The light scattering ability of $TiO_2$ films was also visually observed, as shown in the photographs of the neat NC and DS-$TiO_2$ on NC photoanodes in Figure 5b. When the DS-$TiO_2$ layer was deposited onto the NC-$TiO_2$ layer, the photoelectrodes became more opaque, demonstrating their enhanced light scattering properties. The degree of transparency of the photoanodes was significantly reduced upon using DS2 or DS3, which is consistent with the light reflectance results.

IPCE is defined as the ratio of the number of electrons in the external circuit produced by incident photons to the number of generated charge carriers at a given wavelength. Thus, the light scattering effect can be evaluated by measuring the IPCE spectra of $TiO_2$ photoanodes. The IPCE spectra of the qssDSSCs fabricated with a nanogel electrolyte and various photoanodes were measured at AM 1.5 as a function of the illumination wavelength, as shown in Figure 6a. The IPCE values of qssDSSCs fabricated with DS-$TiO_2$ on the NC layer were always higher than that of the NC-only layer over the entire wavelength range from 400 to 800 nm, indicating the crucial role of DS-$TiO_2$ as a top layer to improve the DSSC performance. The highest IPCE value at a wavelength of 525

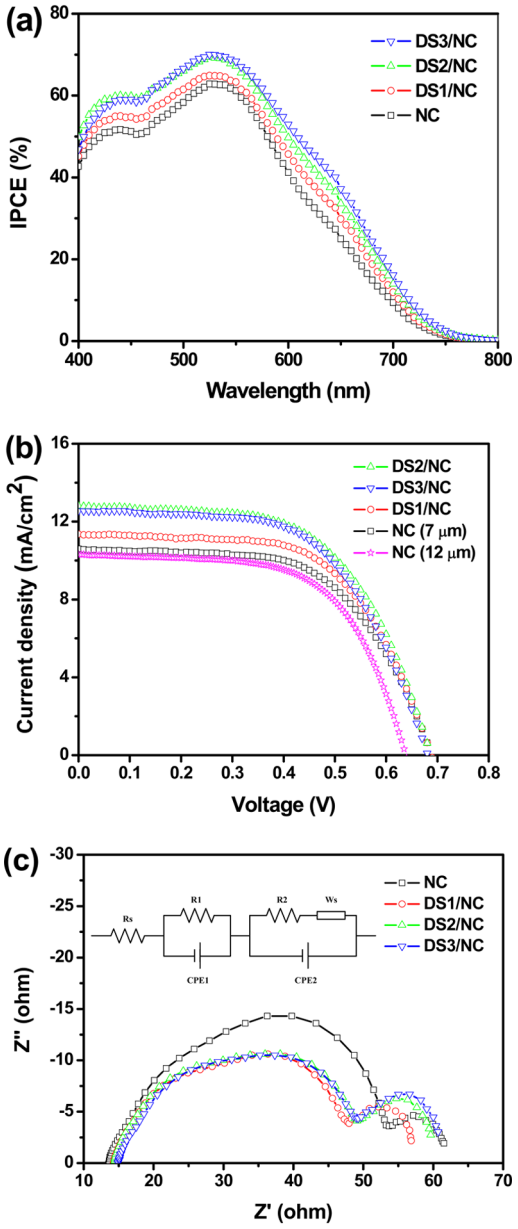


**Figure 6.** (a) IPCE curves, (b) current density and voltage (J-V) curves, and (c) Nyquist plots of qssDSSCs fabricated with a nanogel electrolyte and the different photoanodes under one sun illumination conditions (100 mW/cm$^2$); the inset image of (c) is the equivalent circuit.

nm results from the absorption peak of the N719 dye, assigned to the visible $t_2$ to $\pi^*$ metal to ligand charge transfer.[21] The enhancement of IPCE value at wavelengths shorter than 525 nm results from the dye adsorption amount, whereas that at wavelengths longer than 525 nm is the result of the light scattering efficiency. Double-layer qssDSSCs exhibited higher IPCE values at both shorter (<525 nm) and longer wavelengths (>525 nm), which is indicative of enhancements in both dye loading and light scattering properties, which is consistent with the dye adsorption measurement and light reflectance spectra. In order to clearly represent the effect of DS-$TiO_2$ on the light scattering effect, the normalized IPCE curves were also plotted by dividing the IPCE data by maximum IPCE value at 525 nm (Figure S3). The DS/NC $TiO_2$ photoanodes markedly enhanced the IPCE values compared to those of the pristine NC $TiO_2$ in the longer wavelength region of 525−800 nm, demonstrating the strong scattering effect of DS-$TiO_2$ over the visible light range.

The ssDSSCs and qssDSSCs are more advantageous than the liquid electrolyte-based counterpart due to the need for long-term stability, a flexible design, and lightweight cells. The qssDSSCs were fabricated with a nanogel electrolyte and various $TiO_2$ photoanodes, and the resulting J-V curves were measured at 100 mW/cm$^2$, as shown in Figure 6b. The performance parameters including the $J_{sc}$, $V_{oc}$, FF, and $\eta$ values are summarized in Table 1. The nanogel electrolyte consisted of poly(ethylene glycol) dimethyl ether (PEGDME), 1-methyl-3-propylimidazolium iodide (MPII), fumed silica, and iodine ($I_2$). Overall, the $V_{oc}$ and FF values of the qssDSSCs with and without DS-$TiO_2$ as the scattering top layer were not significantly different from each other, producing $V_{oc}$ values in the range of 0.68−0.69 and FF values in the range of 0.57−0.58. These results demonstrate that the introduction of DS-$TiO_2$ as a top scattering layer did not have a negative effect on the pore-filling of the electrolyte. This may be due to the large interstitial void spaces of DS-$TiO_2$, which allow for the electrolytes to penetrate well into the pores. The $J_{sc}$ values of the qssDSSCs with a DS-$TiO_2$ scattering layer were always higher than that of only NC-$TiO_2$ due to increased dye adsorption and the enhanced light scattering effect, as confirmed by the dye loading measurements, light reflectance spectra, and IPCE curves. In particular, DS2 on the NC layer achieved the highest conversion efficiency and $J_{sc}$ values of 5.0% and 12.9 mA/cm$^2$, respectively, which are approximately 19% higher than those of NC. Thus, the DS-$TiO_2$ layer could play an important role in the enhancement of the $J_{sc}$ value by increasing the light scattering ability and dye adsorption without any negative impact on the $V_{oc}$ or FF value. The efficiency of DS3/NC $TiO_2$ reached 4.9%, which is not significantly different from that of DS2/NC $TiO_2$. This similarity is attributed to the similar values of dye loading and light reflecting properties between DS3/NC and DS3/NC, implying the achievement of critical film thickness and DS-$TiO_2$ size.

EIS measurements were carried out to demonstrate the effects of the DS-$TiO_2$ layer on the performance of DSSCs. The EIS Nyquist plots of the qssDSSCs with a nanogel electrolyte and various $TiO_2$ photoanodes were measured at open circuit under one sun illumination, as shown in Figure 6c. Internal/interfacial impedances were determined by fitting experimental data with an equivalent circuit, consisting of an Ohmic series resistance of the substrate ($R_S$, starting point of the first semicircle in the Nyquist plot), charge transport resistance at the Pt counter electrode and $TiO_2$ photoanode/dye/electrolyte ($R_{ct}$, first two semicircles in the EIS Nyquist plot), Warburg diffusion in the electrolyte ($W_s$, third semicircle in the EIS Nyquist plot), and a constant phase element of capacitance corresponding to $R_1$ (CPE1) and $R_2$ (CPE2).[39] Here, we focused on the second semicircle of the Nyquist plot in order to investigate the charge transfer characteristics at the $TiO_2$ photoanode/dye/electrolyte. As shown in Table 2, the $R_2$ values determined from the real component of the qssDSSC with a DS-$TiO_2$ layer (33.7 Ω, 34.7 Ω, and 34.1 Ω for DS1, DS2, and DS3, respectively) were always smaller than that of NC-based qssDSSC (40.1 Ω). This result is due to the well-organized 2D structure, high porosity, and large interstitial pores of the DS-$TiO_2$ layer to allow facile pore-filling of

**Table 2. EIS Parameters of qssDSSCs with NC, DS1/NC, DS2/NC, and DS3/NC Photoanodes**

| photoanode | $R_s$ (Ω) | $R_{ct}$ (Ω) | $W_s$ (Ω) |
|---|---|---|---|
| NC | 13.57 | 40.09 | 7.86 |
| DS1/NC | 14.21 | 33.65 | 8.90 |
| DS2/NC | 14.26 | 34.72 | 10.53 |
| DS3/NC | 14.88 | 34.06 | 11.46 |

electrolyte, which facilitates efficient ion transport and dye regeneration.

The double-layer photoanode consisting of 2.5-$\mu$m-thick DS-$TiO_2$ on 7.0-$\mu$m-thick NC-$TiO_2$ was also utilized to fabricate ssDSSCs with a PIL. PEBII with a molecular weight of 15 000 g/mol was synthesized via free radical polymerization and was employed as a solid PIL for ssDSSCs. PEBII functions well as an electrolyte without any additives such as iodide salt, ionic liquid, or iodine ($I_2$).[39,40] As shown in Figure 7, the efficiency of

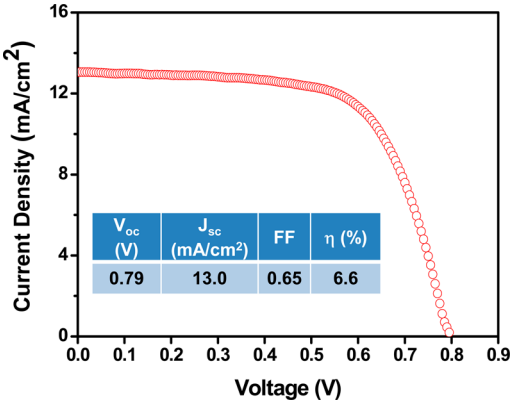


**Figure 7.** J-V curve of the ssDSSC fabricated with two layers and a solid PEBII electrolyte at 100 mW/cm$^2$.

the ssDSSC with PEBII reached 6.6% at 100 mW/cm$^2$, which is larger than that of the qssDSSCs and among the higher values reported for N719 dye-based solid electrolyte DSSCs.[8−10,36−41,46,47] The higher efficiency of the PEBII-based ssDSSC results from the higher mobility of PEBII due to a well-organized, pi-pi stacking structure and lower glass transition temperature.[39] This result demonstrates that the bifunctional DS-$TiO_2$ layer with a 2D structure and anatase phase allows the reflection/or scattering of the unabsorbed photons back into the device and also provides additional surface area for improved dye adsorption. Both factors contribute to enhanced light harvesting and therefore improved $J_{sc}$ value of DSSCs without any negative impact on the $V_{oc}$ or FF value.

## CONCLUSION

In this study, we first report disk-shaped $TiO_2$ with a 2D structure and anatase phase synthesized by a facile method using only TTIP, EC, and a solvent. We demonstrated that the use of EC and a THF/toluene mixture as a polymer template and solvent, respectively, are key factors for generating such nanostructures. More importantly, the DS-$TiO_2$ was able to be directly deposited onto a NC-$TiO_2$ film with a thickness of 1.5−3.5 $\mu$m, implying that it is possible to apply the structure to a light scattering layer. The size of the anatase DS-$TiO_2$ particles ranged from 500 nm to 2 $\mu$m and gradually increased with increasing amount of TTIP, as characterized by FE-SEM, EF-TEM, and XRD analyses. The introduction of the DS-$TiO_2$ layer onto the NC-$TiO_2$ film resulted in an improved energy conversion efficiency from 4.2 to 5.0% for the qssDSSCs at 100 mW/cm$^2$ without any $TiCl_4$ post-treatment. The improved performance is mostly due to the enhanced $J_{sc}$ value resulting from the improved dye loading and light scattering ability of the DS-$TiO_2$ layer, as confirmed by UV−visible reflectance spectra and IPCE measurements. A high efficiency (6.6% at 100 mW/cm$^2$) was also obtained by utilizing double-layer structures and a solid PIL as a photoelectrode and electrolyte, respectively. The efficiency improvements resulted from the combination of high mobility of PEBII as a solid PIL and a bifunctional DS-$TiO_2$ layer with a 2D structure and anatase phase. We believe that the EC-directed approach based on control of polymer−solvent interaction introduces a new and inexpensive route for the synthesis of well-organized, 2D disk-shaped nanostructures as an alternative to the conventional hydrothermal reaction that requires high temperature and pressure.

## ASSOCIATED CONTENT

### Supporting Information

Photographs of DS-$TiO_2$ sol−gel mixtures, EF-TEM images of DS-$TiO_2$ and normalized IPCE curves. This material is available free of charge via the Internet at http://pubs.acs.org.

## AUTHOR INFORMATION

### Corresponding Author

*Phone: 82-2-2123-5757. Fax: 82-2-312-6401. E-mail: jonghak@yonsei.ac.kr.

### Notes

The authors declare no competing financial interest.

## ACKNOWLEDGMENTS

This work was supported by the Korea Center for Artificial Photosynthesis (KCAP) (2009-0093883), the Core Research Program (2012R1A2A2A02011268), and the Energy Efficiency & Resources of the Korea Institute of Energy Technology Evaluation and Planning (KETEP) (20122010100040).

## REFERENCES

(1) O'Regan, B.; Gratzel, M. A Low-Cost, High-Efficiency Solar Cell Based on Dye-Sensitized Colloidal $TiO_2$ Films. *Nature* **1991**, *353*, 737−740.

(2) Chen, C.-Y.; Chen, J.-G.; Wu, S.-J.; Li, J.-Y.; Wu, C.-G.; Ho, K.-C. Multifunctionalized Ruthenium-Based Supersensitizers for Highly Efficient Dye-Sensitized Solar Cells. *Angew. Chem., Int. Ed.* **2008**, *47*, 7342−7345.

(3) Desai, U. V.; Xu, C.; Wu, J.; Gao, D. Hybrid $TiO_2$−$SnO_2$ Nanotube Arrays for Dye-Sensitized Solar Cells. *J. Phys. Chem. C* **2013**, *117*, 3232−3239.

(4) Wu, W.-Q.; Feng, H.-L.; Rao, H.-S.; Xu, Y.-F.; Kuang, D.-B.; Su, C.-Y. Maximizing Omnidirectional Light Harvesting in Metal Oxide Hyperbranched Array Architectures. *Nat. Commun.* **2014**, *5*, 3968.

(5) Huang, F.; Chen, D.; Chen, Y.; Caruso, R. A.; Cheng, Y.-B. Mesoporous Titania Beads for Flexible Dye-Sensitized Solar Cells. *J. Mater. Chem. C* **2014**, *2*, 1284−1289.

(6) Wu, W.-Q.; Xu, Y.-F.; Rao, H.-S.; Feng, H.-L.; Su, C.-Y.; Kuang, D.-B. Constructing 3D Branched Nanowire Coated Macroporous Metal Oxide Electrodes with Homogeneous or Heterogeneous Compositions for Efficient Solar Cells. *Angew. Chem., Int. Ed.* **2014**, *53*, 4816−4821.

(7) Krishnamoorthy, T.; Tang, M. Z.; Verma, A.; Nair, A. S.; Pliszka, D.; Mhaisalkar, S. G.; Ramakrishna, S. A Facile Route to Vertically Aligned Electrospun $SnO_2$ Nanowires on a Transparent Conducting

Oxide Substrate for Dye-Sensitized Solar Cells. *J. Mater. Chem.* **2012**, *22*, 2166−2172.
(8) Xia, J.; Masaki, N.; Lira-Cantu, M.; Kim, Y.; Jiang, K.; Yanagida, S. Influence of Doped Anions on Poly(3,4-ethylenedioxythiophene) as Hole Conductors for Iodine-Free Solid-State Dye-Sensitized Solar Cells. *J. Am. Chem. Soc.* **2008**, *130*, 1258−1263.
(9) Wang, H.; Zhang, X.; Gong, F.; Zhou, G.; Wang, Z.-S. Novel Ester-Functionalized Solid-State Electrolyte for Highly Efficient All-Solid-State Dye-Sensitized Solar Cells. *Adv. Mater.* **2012**, *24*, 121−124.
(10) Chu, T.-C.; Lin, R. Y.-Y.; Lee, C.-P.; Hsu, C.-Y.; Shih, P.-C.; Lin, R.; Li, S.-R.; Sun, S.-S.; Lin, J. T.; Vittal, R.; Ho, K.-C. Ionic Liquid with a Dual-Redox Couple for Efficient Dye-Sensitized Solar Cells. *ChemSusChem* **2014**, *7*, 146−153.
(11) Roy-Mayhew, J. D.; Bozym, D. J.; Punckt, C.; Aksay, I. A. Functionalized Graphene as a Catalytic Counter Electrode in Dye-Sensitized Solar Cells. *ACS Nano* **2010**, *4*, 6203−6211.
(12) Park, Y.-C.; Chang, Y.-J.; Kum, B.-G.; Kong, E.-H.; Son, J. Y.; Kwon, Y. S.; Park, T.; Jang, H. M. Size-Tunable Mesoporous Spherical $TiO_2$ as a Scattering Overlayer in High-Performance Dye-Sensitized Solar Cells. *J. Mater. Chem.* **2011**, *21*, 9582−9586.
(13) Trang Pham, T. T.; Bessho, T.; Mathews, N.; Zakeeruddin, S. M.; Lam, Y. M.; Mhaisalkar, S.; Gratzel, M. Light Scattering Enhancement from Sub-Micrometer Cavities in the Photoanode for Dye-Sensitized Solar Cells. *J. Mater. Chem.* **2012**, *22*, 16201−16204.
(14) Passoni, L.; Ghods, F.; Docampo, P.; Abrusci, A.; Martí-Rujas, J.; Ghidelli, M.; Divitini, G.; Ducati, C.; Binda, M.; Guarnera, S.; Li Bassi, A.; Casari, C. S.; Snaith, H. J.; Petrozza, A.; Di Fonzo, F. Hyperbranched Quasi-1D Nanostructures for Solid-State Dye-Sensitized Solar Cells. *ACS Nano* **2013**, *7*, 10023−10031.
(15) Chen, D.; Huang, F.; Cheng, Y.-B.; Caruso, R. A. Mesoporous Anatase $TiO_2$ Beads with High Surface Areas and Controllable Pore Sizes: A Superior Candidate for High-Performance Dye-Sensitized Solar Cells. *Adv. Mater.* **2009**, *21*, 2206−2210.
(16) Sauvage, F.; Chen, D.; Comte, P.; Huang, F.; Heiniger, L.-P.; Cheng, Y.-B.; Caruso, R. A.; Graetzel, M. Dye-Sensitized Solar Cells Employing a Single Film of Mesoporous $TiO_2$ Beads Achieve Power Conversion Efficiencies over 10%. *ACS Nano* **2010**, *4*, 4420−4425.
(17) Huang, F.; Chen, D.; Zhang, X. L.; Caruso, R. A.; Cheng, Y.-B. Dual-Function Scattering Layer of Submicrometer-Sized Mesoporous $TiO_2$ Beads for High-Efficiency Dye-Sensitized Solar Cells. *Adv. Funct. Mater.* **2010**, *20*, 1301−1305.
(18) Roh, D. K.; Seo, J. A.; Chi, W. S.; Koh, J. K.; Kim, J. H. Facile Synthesis of Size-Tunable Mesoporous Anatase $TiO_2$ Beads Using a Graft Copolymer for Quasi-Solid and All-Solid Dye-Sensitized Solar Cells. *J. Mater. Chem.* **2012**, *22*, 11079−11085.
(19) Xue, X.; Tian, J.; Liao, W.; Shan, Z. Spherical Anatase $TiO_2$ Covered with Nanospindles as Dual Functional Scatters for Dye-Sensitized Solar Cells. *Electrochim. Acta* **2014**, *123*, 463−469.
(20) Kim, K. S.; Song, H.; Nam, S. H.; Kim, S.-M.; Jeong, H.; Kim, W. B.; Jung, G. Y. Fabrication of an Efficient Light-Scattering Functionalized Photoanode Using Periodically Aligned ZnO Hemisphere Crystals for Dye-Sensitized Solar Cells. *Adv. Mater.* **2012**, *24*, 792−798.
(21) Dong, Z.; Ren, H.; Hessel, C. M.; Wang, J.; Yu, R.; Jin, Q.; Yang, M.; Hu, Z.; Chen, Y.; Tang, Z.; Zhao, H.; Wang, D. Quintuple-Shelled $SnO_2$ Hollow Microspheres with Superior Light Scattering for High-Performance Dye-Sensitized Solar Cells. *Adv. Mater.* **2014**, *26*, 905−909.
(22) Tiwana, P.; Docampo, P.; Johnston, M. B.; Snaith, H. J.; Herz, L. M. Electron Mobility and Injection Dynamics in Mesoporous ZnO, $SnO_2$, and $TiO_2$ Films Used in Dye-Sensitized Solar Cells. *ACS Nano* **2011**, *5*, 5158−5166.
(23) Qian, J.; Liu, P.; Xiao, Y.; Jiang, Y.; Cao, Y.; Ai, X.; Yang, H. $TiO_2$-Coated Multilayered $SnO_2$ Hollow Microspheres for Dye-Sensitized Solar Cells. *Adv. Mater.* **2009**, *21*, 3663−3667.
(24) Lei, B.-X.; Zeng, L.-L.; Zhang, P.; Qiao, H.-K.; Sun, Z.-F. Sugar Apple-Shaped $TiO_2$ Hierarchical Spheres for Highly Efficient Dye-Sensitized Solar Cells. *J. Power Sources* **2014**, *253*, 269−275.
(25) Seo, J. A.; Roh, D. K.; Koh, J. K.; Kim, S. J.; Jung, B.; Kim, J. H. Low Temperature Synthesis of Flower-Like $TiO_2$ Nanospheres Directly from Block-Graft Copolymer Precursors and Their Uses in Quasi-Solid-State Dye-Sensitized Solar Cells. *Electrochim. Acta* **2012**, *80*, 27−33.
(26) Zhu, K.; Neale, N. R.; Miedaner, A.; Frank, A. J. Enhanced Charge-Collection Efficiencies and Light Scattering in Dye-Sensitized Solar Cells Using Oriented $TiO_2$ Nanotubes Arrays. *Nano Lett.* **2006**, *7*, 69−74.
(27) Jennings, J. R.; Ghicov, A.; Peter, L. M.; Schmuki, P.; Walker, A. B. Dye-Sensitized Solar Cells Based on Oriented $TiO_2$ Nanotube Arrays: Transport, Trapping, and Transfer of Electrons. *J. Am. Chem. Soc.* **2008**, *130*, 13364−13372.
(28) Han, S.-H.; Lee, S.; Shin, H.; Suk, J. H. A Quasi-Inverse Opal Layer Based on Highly Crystalline $TiO_2$ Nanoparticles: A New Light-Scattering Layer in Dye-Sensitized Solar Cells. *Adv. Energy Mater.* **2011**, *1*, 546−550.
(29) Liu, B.; Aydil, E. S. Growth of Oriented Single-Crystalline Rutile $TiO_2$ Nanorods on Transparent Conducting Substrates for Dye-Sensitized Solar Cells. *J. Am. Chem. Soc.* **2009**, *131*, 3985−3990.
(30) Barea, E.; Xu, X.; Gonzalez-Pedro, V.; Ripolles-Sanchis, T.; Fabregat-Santiago, F.; Bisquert, J. Origin of Efficiency Enhancement in $Nb_2O_5$ Coated Titanium Dioxide Nanorod Based Dye Sensitized Solar Cells. *Energy Environ. Sci.* **2011**, *4*, 3414−3419.
(31) Heo, S. Y.; Kim, D. J.; Jeon, H.; Jung, B.; Kang, Y. S.; Kim, J. H. Vertically Aligned Anatase $TiO_2$ Nanotubes on Transparent Conducting Substrates Using Polycarbonate Membranes. *RSC Adv.* **2013**, *3*, 13681−13684.
(32) Roh, D. K.; Patel, R.; Ahn, S. H.; Kim, D. J.; Kim, J. H. Preparation of $TiO_2$ Nanowires/nanotubes Using Polycarbonate Membranes and Their Uses in Dye-Sensitized Solar Cells. *Nanoscale* **2011**, *3*, 4162−4169.
(33) Feng, X.; Shankar, K.; Varghese, O. K.; Paulose, M.; Latempa, T. J.; Grimes, C. A. Vertically Aligned Single Crystal $TiO_2$ Nanowire Arrays Grown Directly on Transparent Conducting Oxide Coated Glass: Synthesis Details and Applications. *Nano Lett.* **2008**, *8*, 3781−3786.
(34) Krishnamoorthy, T.; Thavasi, V.; Subodh, G. M.; Ramakrishna, S. A First Report on the Fabrication of Vertically Aligned Anatase $TiO_2$ Nanowires by Electrospinning: Preferred Architecture for Nanostructured Solar Cells. *Energy Environ. Sci.* **2011**, *4*, 2807−2812.
(35) Chen, H.-Y.; Kuang, D.-B.; Su, C.-Y. Hierarchically Micro/nanostructured Photoanode Materials for Dye-Sensitized Solar Cells. *J. Mater. Chem.* **2012**, *22*, 15475−15489.
(36) Ahn, S. H.; Chi, W. S.; Park, J. T.; Koh, J. K.; Roh, D. K.; Kim, J. H. Direct Assembly of Preformed Nanoparticles and Graft Copolymer for the Fabrication of Micrometer-Thick, Organized $TiO_2$ Films: High Efficiency Solid-State Dye-Sensitized Solar Cells. *Adv. Mater.* **2012**, *24*, 519−522.
(37) Ahn, S. H.; Kim, D. J.; Chi, W. S.; Kim, J. H. One-Dimensional Hierarchical Nanostructures of $TiO_2$ Nanosheets on $SnO_2$ Nanotubes for High Efficiency Solid-State Dye-Sensitized Solar Cells. *Adv. Mater.* **2013**, *25*, 4893−4897.
(38) Ahn, S. H.; Park, J. T.; Koh, J. K.; Roh, D. K.; Kim, J. H. Graft Copolymer Directed Synthesis of Micron-Thick Organized Mesoporous $TiO_2$ Films for Solid-State Dye-Sensitized Solar Cells. *Chem. Commun.* **2011**, *47*, 5882−5884.
(39) Park, J. T.; Chi, W. S.; Roh, D. K.; Ahn, S. H.; Kim, J. H. Hybrid Templated Synthesis of Crack-Free, Organized Mesoporous $TiO_2$ Electrodes for High Efficiency Solid-State Dye-Sensitized Solar Cells. *Adv. Funct. Mater.* **2013**, *23*, 26−33.
(40) Chi, W. S.; Roh, D. K.; Kim, S. J.; Heo, S. Y.; Kim, J. H. Hybrid Electrolytes Prepared from Ionic Liquid-Grafted Alumina for High-Efficiency Quasi-Solid-State Dye-Sensitized Solar Cells. *Nanoscale* **2013**, *5*, 5341−5348.
(41) Koh, J. K.; Kim, J.; Kim, B.; Kim, J. H.; Kim, E. Highly Efficient, Iodine-Free Dye-Sensitized Solar Cells with Solid-State Synthesis of Conducting Polymers. *Adv. Mater.* **2011**, *23*, 1641−1646.

(42) Laschat, S.; Baro, A.; Steinke, N.; Giesselmann, F.; Hägele, C.; Scalia, G.; Judele, R.; Kapatsina, E.; Sauer, S.; Schreivogel, A.; Tosoni, M. Discotic Liquid Crystals: From Tailor-Made Synthesis to Plastic Electronics. *Angew. Chem., Int. Ed.* **2007**, *46*, 4832−4887.
(43) Bisoyi, H. K.; Kumar, S. Discotic Nematic Liquid Crystals: Science and Technology. *Chem. Soc. Rev.* **2010**, *39*, 264−285.
(44) Wang, L.; Huang, Y. Disklike Texture of Ethyl−Cyanoethyl Cellulose Cholesteric Phase. *Macromolecules* **2002**, *35*, 3111−3116.
(45) Jarvis, M. Cellulose Stacks Up. *Nature* **2003**, *426*, 611−612.
(46) Xu, C.; Wu, J.; Desai, U. V.; Gao, D. High-Efficiency Solid-State Dye-Sensitized Solar Cells Based on $TiO_2$-Coated ZnO Nanowire Arrays. *Nano Lett.* **2012**, *12*, 2420−2424.
(47) Docampo, P.; Guldin, S.; Stefik, M.; Tiwana, P.; Orilall, M. C.; Hüttner, S.; Sai, H.; Wiesner, U.; Steiner, U.; Snaith, H. J. Control of Solid-State Dye-Sensitized Solar Cell Performance by Block-Copolymer-Directed $TiO_2$ Synthesis. *Adv. Funct. Mater.* **2010**, *20*, 1787−1796.